Molecular BioSystems

Dynamic Article Links ►

Cite this: DOI: 10.1039/c0xx00000x

www.rsc.org/xxxxxx

PAPER

Molecular Dynamics and Tubulin Polymerization Kinetics Study on 1,14-Heterofused Taxanes: Evidences of Stabilization of the Tubulin Head-to-Tail Dimer-Dimer Interaction

Alessandro Contini,[a,‡,*] Graziella Cappelletti,[b,‡] Daniele Cartelli,[b] Gabriele Fontana[c] and Maria Luisa Gelmi[a]

Received (in XXX, XXX) Xth XXXXXXXXX 20XX, Accepted Xth XXXXXXXXX 20XX
DOI: 10.1039/b000000x

The effects on tubulin dynamics of paclitaxel, ortataxel and two recently developed taxol derivatives bearing a five-membered heterocyclic ring fused at the 1,14 position were analysed by means of molecular dynamic simulations and MMPBSA approach. Tubulin polymerization kinetics and microtubule morphology assays were also conducted, providing support to computational results. In particular, it has been shown that the two recently developed 1,14-heterofused taxanes IDN5839 and IDN5798 are able to speed up the in vitro tubulin assembly by promoting the nucleation phase and to affect microtubule network in cell earlier than paclitaxel.

Introduction

The microtubule-targeted drug paclitaxel (Taxol®, **1**, Figure 1) is widely used in clinical practice for cancer therapy.[1]

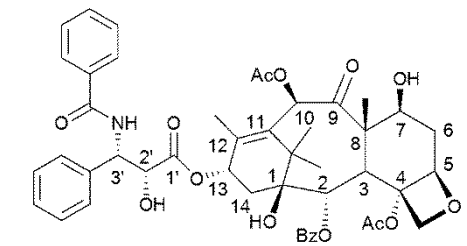

paclitaxel (**1**)

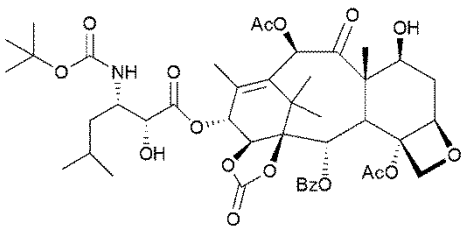

ortataxel (**2**)

Figure 1. Paclitaxel (**1**) and ortataxel (**2**)

Nevertheless, the research of analogues endowed by a more favourable pharmacological profile, in terms of selectivity and tolerability, is still necessary.

Structure-activity studies of several research groups leaded to the observation that changes to the "southern hemisphere", comprising the C14 and C1 to C5 positions, exert a major effect on paclitaxel activity.[2,3] As a demonstration, the potent anticancer taxoid ortataxel (**2**, Figure 1), was prepared starting from 14β-hydroxyl-10-deacetylbaccatin III 1,14-carbonate, a semi-synthetic intermediate obtained from the naturally abundant 10-deacetyl baccatin III.[4] Ortataxel displays improved pharmacological properties, such as a remarkably higher oral bioavailability than paclitaxel and entered clinical trials where it showed a strong activity in Phase II studies on heavily pre-treated metastatic breast and non-small cell lung cancer.[5] To further improve the pharmacological properties of ortataxel, new C14 isosters were recently prepared by our research group.[6]

The development of highly active derivatives takes unquestionable advantages by the knowledge of bioactive conformations (Figure 2).

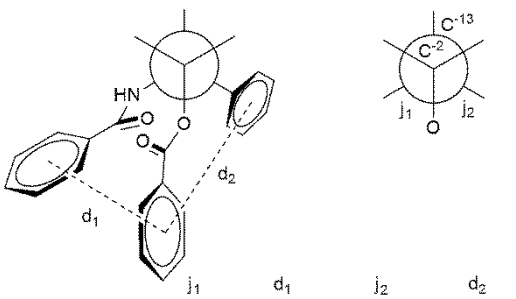

	j_1	d_1	j_2	d_2
Ia non-polar	42°	4.7 Å	-85°	9.8 Å
Ib polar	28°	5.7 Å	-52°	11.6 Å
Ic T-taxol	80°	9.4 Å	-58°	10.0 Å

Figure 2. Proposed bioactive conformations for paclitaxel

The binding conformation of taxol and its derivatives has been the object of several investigations. A bioactive non-polar conformation Ia, showing the clustering of the C2 benzoate and

the C3' benzamido group, was proposed by single conformation NMR studies in apolar solvents,[7] while analogous NMR investigations conducted in polar solvents suggested the hydrophobically collapsed "polar" conformation Ib.[8] However, most of the constrained taxol mimic designed upon both the non-polar and the polar conformations resulted less potent than taxol itself.[9] The T-taxol conformation Ic, supported by theoretical models derived from electron crystallographic density studies as well as by several experimental observations based on constrained taxol analogues,[10] was finally proposed as the bioactive conformation.[11]

Concerning taxol derivatives, the binding modes of IDN5390 (a seco-derivative of taxol) and epothilone A to type I and III isoforms of β-tubulin were investigated by means of restrained molecular dynamic (MD) simulations, providing structural insights about the recognition mode of those antimitotics.[12]

MD simulations were also conducted on a microtubule fragment model (two parallel protofilaments formed by two α and one β subunit) both in presence and absence of paclitaxel,[13] revealing through a root-mean-square-fluctuation analysis that paclitaxel induces changes in the dynamics of the loops surrounding the taxol binding site. The authors suggested that such changes, by affecting the protofilament flexibility, favour the interactions between adjacent protofilaments. Variations in the dynamics at the β-α interface were also observed, but no details were given on the process thermodynamics and, consequently, on the eventual stabilization of the head-to-tail interaction between tubulin dimers in a single protofilament.

In the present work we investigated the binding mode and the interaction energies for tubulin complexes of ortataxel (**2**) and the recently developed 1,14-heterofused taxanes IDN5839 (**3**) and IDN5798 (**4**) represented in Figure 3.

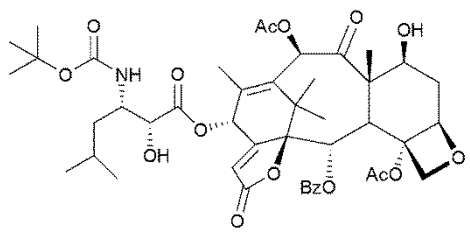

IDN5839 (**3**)

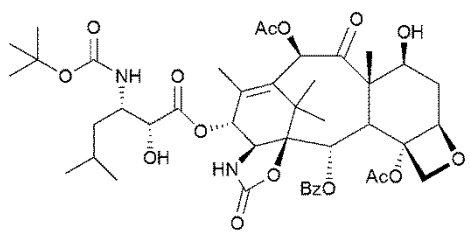

IDN5798 (**4**)

Figure 3. 1,14-Heterofused taxanes analysed in the present study.

Paclitaxel was also included in the study for comparison and to test the reliability of our computational approach. Potential binding geometries for **1**-**4** were generated and then evaluated by MD simulations and molecular mechanics/Poisson Boltzmann surface area (MM-PBSA) calculations.

Moreover, the long range effects of taxanes binding on residues at the 1α-2β interface were evaluated on 1β,1α-2β,2α tubulin tetramers by MD and MM-PBSA calculations, a method that proved to be successful in designing peptides interfering with the dimer-dimer interaction of tubulin,[14] and per-residue free energy decomposition analysis.

Finally, experiments on tubulin polymerization kinetics and on microtubule morphology were also conduced, and the comparison between theoretical and experimental findings revealed significant differences in the biochemical behaviour of the investigated 1,14-heterofused taxanes.

Results and Discussion

Computational Study.

Binding mode and binding energy analysis. Although the structure of the α,β-tubulin dimer complexed with 1 has been determined by electron crystallography at 3.5 Å,[15] it lacks the necessary resolution to define the binding conformation of **1** itself. Despite this, the T-taxol bioactive conformation has been widely supported by binding studies with highly active constrained analogues[10a,d] and REDOR NMR experiments.[11c] To our knowledge, no information are available upon the bioactive conformation of 1,14-heterofused taxanes **2**-**4**, and the assumption of an analogue binding mode with **1** might be dangerous due to the differences at the 1,14 positions and in the side-chain, which bears a t-butylcarbamate and a sec-butyl instead of benzamide and phenyl groups.

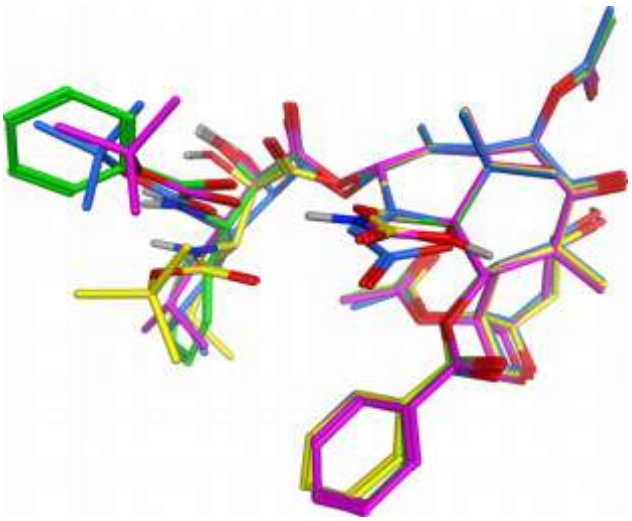

Figure 4. Superposed Lowest energy conformations obtained for the unbounded taxanes 1-4 by low-mode MD conformational search with the MMFF94x force field and Born solvation. **1** (green), **2** (yellow), **3** (cyan), **4** (magenta). Lowest energy conformations obtained for the unbounded taxanes by low-mode MD conformational search with the MMFF94x force field and Born solvation.

A conformational search of unbounded compounds **2**-**4** was then performed using the low mode MD algorithm and the MMFF94x force field with Born solvation for water, implemented in the MOE software.[16] Paclitaxel **1** was also included and the obtained conformation showed for this compound a geometry highly consistent with the REDOR-NMR supported T-taxol conformation.[11c] Compounds **2**-**4** also provided

comparable conformations, as shown by Figure 4 where the lowest energy conformations are superposed. Due to the structural differences in the side-chain and in the 1,14 region, the obtained conformation for **2**-**4** will be hereafter referred as pseudo-T-taxol. It should be noted that, in the superposed geometries represented in Figure 4, the side-chain *tert*-butoxycarbonyl groups of compounds **3** and **4** and the side-chain benzoyl group of **1** are closely matched, while compound **2** shows an higher deviation (computed r.m.s.d. between the amidic carbonyl groups of **2**, **3** and **4** compared to **1** are 0.14, 0.11, 0.12 Å, respectively). Although, by considering all the common heavy atoms in r.m.s.d. calculation between compounds **1** and **2**-**4**, the closest match with **1** is observed for compound **2** (r.m.s.d. = 2.83 Å) followed by **4** and **3** (r.m.s.d. = 3.79 and 3.85Å, respectively).

In order to evaluate the stability of the obtained conformations within the binding environment, complexes were realized by manually docking said conformations of **1**-**4** into the β subunit of a tubulin dimer model derived from the 1JFF crystal structure.[15] The complexes were processed by MD simulations in explicit water and, after a careful equilibration, a 2 ns production run was performed, a length considered adequate in similar and recently published studies.[14]

In order to verify the possibility of alternative binding conformations, different starting complexes were also generated by automated docking, using two different protocols previously optimized in order to reproduce at best the experimentally determined binding conformation of **1** (see Experimental for details). For each compound, the top five poses of both protocols were used for generating complexes which were subjected to the MD procedure described above. All trajectories were then analysed by MM-PBSA, a reliable method to discriminate different binding conformation by computing free energies of binding on a statistically relevant thermodynamic ensemble.[17] In order to select a proper binding conformation, the MM-PBSA derived complex absolute stabilities and ligand binding energies were both evaluated. Table 1 reports the binding energies obtained for the lowest energy pose (see Table S1, Supporting Information, for full results), together with geometrical parameters selected to provide a common term of comparison between **1** and the 1,14-heterofused taxanes **2**-**4** (Figure 5).

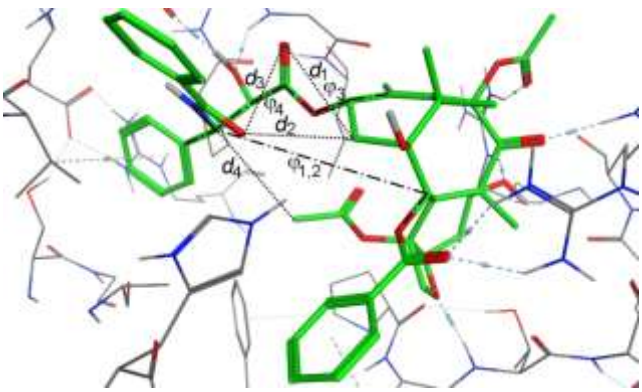

Figure 5. Distances d_1 (C1'=O···C14), d_2 (C14···O=CNH), d_3 (HNC=O···O=C1'), d_4 (C11-OCOCH3···C3'); torsion angles φ_1 and φ_2 (O-C2-C3'-N and O-C2-C3'-C, accordingly to reference 11a), and dihedral angles φ_3 and φ_4 (C12-C13-O-C1' and O-C1'-C2'-C3', respectively, accordingly to reference 11b).

Table 1. Computed MM-PBSA Binding Energies for the Most Favored Pose and Average Geometrical Parameters for the Bounded Taxanes.[a]

	1	**2**	**3**	**4**
$\Delta E_{\text{MM-PBSA}}$	-39.7±7.0	-36.0±5.4	-36.6±5.4	-29.2±4.1
d_1	3.9±0.2	3.9±0.3	3.8±0.2	3.5±0.3
d_2	3.4±0.2	4.5±0.4	4.5±0.4	4.1±0.4
d_3	3.8±0.3	3.8±0.5	3.8±0.4	3.6±0.4
d_4	4.0±0.2	4.2±0.3	4.3±0.3	3.9±0.2
φ_1	76.8±5.8	85.7±9.7	94.2±8.9	61.7±12.2
φ_2	-56.9±7.4	-70.5±13.5	-59.7±9.2	-85.8±14.9
φ_3	-117.5±18.2	-112.3±23.8	-114.0±16.9	-139.7±23.1
φ_4	82.0±14.1	94.7±19.0	92.3±15.4	95.5±14.8

[a] Geometrical parameters averaged upon frames sampled in the final ns trajectory of production run

As expected, the T-taxol conformation provided for **1** the best results in terms of both complex stability and ligand binding energy (Table S1, Paclitaxel(1) t-taxol). The same was observed for **3**, where calculations starting from the pseudo-T-taxol conformation provided the lowest energies in terms of stability and binding energy (Table S1, IDN5839(3) pseudo-T-taxol). Less clean results were obtained for compounds **2** and **4**, where three low energy complexes were obtained for the former (IDN5109(2) 2_1, 2_2 and pseudo-T-taxol), and two for the latter (IDN5798(4) 5_2 and pseudo-T-taxol). However, the pseudo-T-taxol conformation resulted in both cases the most favoured in terms of binding energies, confirming that **1** and the 1,14-heterofused taxanes **2**-**4** adopt similar binding modes.

The analysis of geometrical parameters (Figure 5 and Table 1) showed that d_1, d_3 and d_4 distances are quite conserved, while d_2 distance is evidently longer for 1,14-heterofused taxanes, probably due to the substitution at C14. Concerning selected torsions, describing the side-chain orientation relatively to the main scaffold, a slight widening of φ_1 and φ_4 dihedrals is observed for compounds **2** and **3** with respect to **1**, while only the former shows a widening of φ_2 of about 10 deg. A different behaviour is observed for compound **4**, which presents a narrower φ_1 (61.7±12.2 deg.) and wider φ_2 and φ_3 (-85.8±14.9 and -139.7±23.1, respectively). This behaviour might be due to the strong H-bond that can be formed between the side-chain tert-butyloxycarbonyl and the cyclic NH at C14, which characterizes compound **4**.

The analysis of intermolecular H-bonds between β-tubulin and taxanes **1**-**4** (Table 2) shows interactions with Asp 26', Thr 274' and Arg 282' for all of them. **1** also shows a rather persistent H-bond with Gln 280' and Gly 360', while the neighbouring Arg 359' establishes a quite stable and peculiar H-bond with **3**. Similarly to **1**, **2** also establishes H-bonds with Gln 280' and Gly 360', even if their average occupancy is lower, while no H-bonds are observed for compound **4** with Gln 280', Arg 359' or Gly 360'. It should be noted that an H-bond, even if showing a low average occupancy (8.2%), was also detected between the compound **3** carbonyl of the 1,14 ring and His 227'.

Table 2. H-bond analysis.[a] H-bonds with an average occupancy above 40% for at least one compound are reported

	average occupancy (%)			
H-Bonds	**1**	**2**	**3**	**4**
Asp26'-COO···HN-C3'	93.6	93.3	89.5	57.6
Asp26'-COO···HO-C2'	99.9	92.0	79.6	n.d.
Thr274'-NH···O-C10	96.1	88.5	65.1	26.0
Gln280'-NH_2···O=C6	93.8	9.5	n.d.	n.d.
Arg282'-NH_2···O-C8	17.8	n.d.	58.2	6.5
Arg282'-NH_2···O=C6	n.d.	n.d.	n.d.	46.4
Arg282'-NH_2···OC(CH_3)O-C5	59.6	25.0	17.2	n.d.
Arg359'-NH···O-C2'	n.d.	n.d.	66.9	n.d.
Gly360'-NH···O-C2'	88.1	28.3	n.d.	n.d.

[a] Parameters for H-bond analysis: donor-acceptor distance: 3.5 Å; donor-H-acceptor angle 120.0 deg. The analysis was performed on the last ns of the production run trajectory.

MM-PBSA binding energies are comparable for all the investigated compounds, in line with previously reported results on cytotoxic activity (IC_{50} on MCF7 tumor cell lines for **1**,[18] and **2**, **3**, **4**[19] are 1.7±0.40, 1.6±0.10, 0.4±0.10 and 1.0±0.04 nM, respectively), even if, in discordance with experiments, compound **4** resulted the less favoured.

Analysis of the effects of taxanes at the tubulin 1α-2β interface. Although we did not expect force field methods to discriminate ligands with such a narrow potency interval, the above computational result might conceal a behaviour that goes farther than the simple differences in binding affinity. For this reason, we decided to test the effects of **1**-**4** on the interaction energy between two consecutive tubulin dimers, a closer model of a tubulin protofilament structure.

Table 3. MM-PBSA energy decomposition analysis for the protein-protein interaction between tubulin 1α and 2β subunits evaluated from the MD of 1β,1α-2 β,2α tetramer;[a] single contributions (kcal/mol) for selected amino acids are reported relatively to unbounded tetramer.[b] Total MM-PBSA binding energy ($\Delta E_{binding}$, kcal/mol) for the 1α-2β dimer-dimer interaction is also reported.[c]

		per residue $\Delta\Delta E_{bound\text{-}unbound}$ (kcal/mol)			
Chain	Residue	**1**	**2**	**3**	**4**
1α	Arg2	-0.4	0.0	-3.7	-5.6
1α	Lys163	-0.3	-0.2	-0.6	-4.2
1α	Glu254	-2.1	0.7	-0.2	-2.0
1α	Asp345	-1.1	-1.7	-0.3	-2.0
1α	Pro348	-2.3	-1.1	-1.1	-1.0
1α	Thr349	-0.8	2.0	0.1	-1.6
2β	Glu69'	0.3	0.0	-0.1	-2.4
2β	Arg390'	3.6	2.4	3.5	3.6
2β	Arg391'	2.8	1.7	1.0	0.0
2β	Phe394'	-1.4	-2.4	-0.9	-3.2
$\Delta E_{binding}$		-39.1±5.6	-33.6±8.4	-52.1±6.5	-72.1±6.8

[a] The analysis was performed on the last ns of the production run trajectory. [b] Single residue contribution are computed as the difference between taxane bounded and unbounded tubulin. Only contributions where $|\Delta\Delta E| > 2$ kcal/mol for at least one compound are reported. [c] The $\Delta E_{binding}$ computed for the unbounded tetramer is -39.1±8.0 kcal/mol.

MD simulations were performed on models of the 1β,1α-2β,2α tubulin tetramer, derived from the 3N2G tubulin tetramer crystal structure,[20] unbounded or bounded with **1**-**4** in their most favoured binding poses (Figure S1).

The binding energy between the 1α-2β subunits was then computed and decomposed into single residue contributions by MM-PBSA analysis of the last ns of production run trajectory. Computed relative energies with respect to unbounded tubulin, are reported in Table 3, while the full set of energies is provided as Supporting Information (Table S2).

Unexpectedly, compound **4** provided the highest stabilization of the dimer-dimer interaction (MM-PBSA $\Delta E_{binding}$=-72.1±6.8 kcal/mol), followed by **3** which also provided a significant stabilization with respect to the unbounded tubulin ($\Delta E_{binding}$=-52.1±6.5 and -39.1±8.0 kcal/mol, respectively). On the other hand, neither compound **2** nor **1** significantly affected the 1α-2β interaction energy. These data suggest that the principal microtubule stabilizing action of compounds **1** and **2** might occur by improving the parallel interaction between adjacent protofilaments, as suggested by Mitra and co-workers,[13] while an additional stabilization mechanism, exerted by improving the head-tail dimer-dimer affinity, could be expected for compounds **3** and **4**.

Experimental Study.

In order to assess the interaction of compounds **1**-**4** with the tubulin/microtubule system, they were initially tested in an in vitro tubulin polymerization assay at fixed concentration of 10 μM. As shown by the kinetics of assembly reported in Figure 6A, compounds 1-4 induce tubulin polymerization even in the absence of GTP.

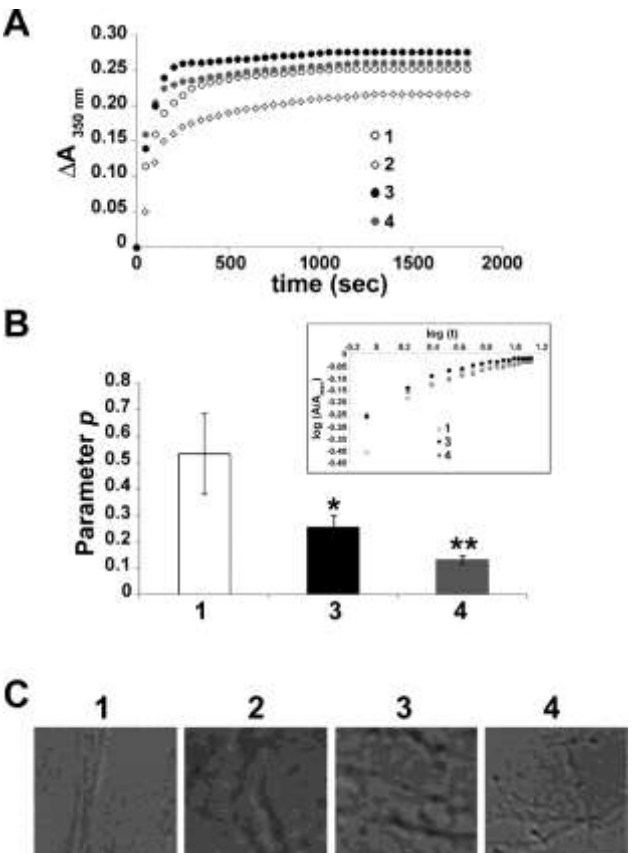

Figure 6. (A) Tubulin assembly was recorded as a function of time by measuring the increase in absorbance at 350 nm. Tubulin (13 μM) was polymerised in assembly buffer without GTP in the presence of compounds **1**-**4** at 10 μM concentrations. (B) Nucleation phase was analysed by extrapolating the parameter p from assembly kinetics, as shown in the inset, obtained in the presence of 1 or compounds 3, 4. (C) DIC microscopy images of microtubules assembled in the presence of compounds **1**-**4** (Bar, 2 μm).

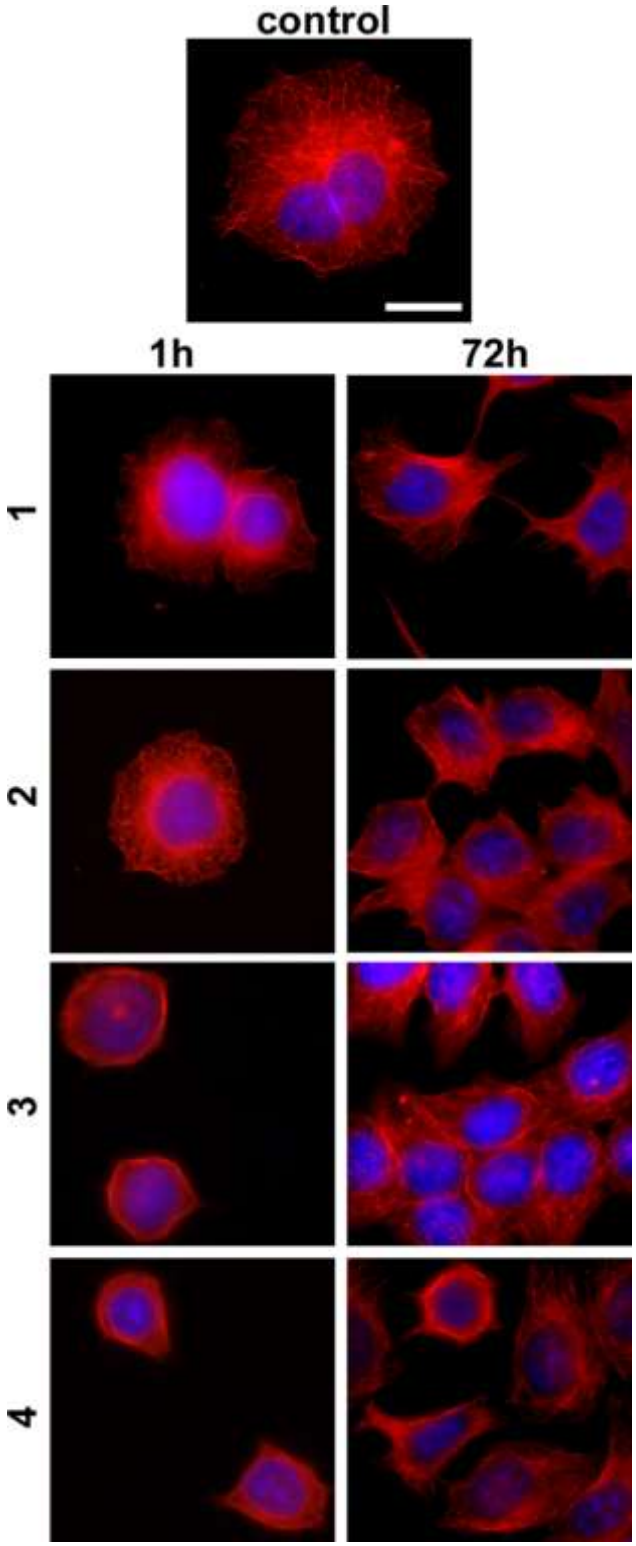

Figure 7. Microtubule organization in human MCF7 cells exposed for 1 and 72 h to compounds **1** (1.7 nM), **2** (1.6 nM), **3** (0.4 nM), and **4** (1 nM), as revealed by immunofluorescence localization of α-tubulin (red). Nuclei are stained by DAPI (blue). Scale bars, 20 μm

However, as the kinetics appear not to be perfectly superposed in the presence of the different compounds, we carried out further analyses to calculate a range of parameters characteristic of the assembly kinetics: nucleation, elongation, and steady state phase. From nucleation phase we extrapolated the parameter *p* (see Experimental Section) and found that it was significantly reduced by the compounds **3** and **4** with respect to **1** (Figure 6B), suggesting these compounds as more effective than **1** in favouring microtubule nucleation.

Table 4. Kinetic parameters of tubulin assembly in the presence of compounds **1-4** (10 μM).

cmpd	V_i ± sem	ΔA ± sem
1	0.074±0.029	0.220±0.052
2	0.081±0.026	0.188±0.018
3	0.159±0.040*	0.235±0.045
4	0.158±0.027*	0.285±0.031

* p<0.05 vs 1 according to ANOVA, Tukey post hoc.

Table 4 reports the maximal velocity of polymerization (Vi) and the steady state extent of assembly (ΔA) extrapolated by the assembly kinetics shown in Figure 6A. Compounds **3** and **4** induce a significant increase in Vi with respect to **1** showing the ability to improve the elongation phase as well as observed above for nucleation. Conversely, the steady state extent of assembly is comparable in the presence of **1** and all the tested compounds. Looking at microtubule morphology, we collected the assembled microtubules at the end of polymerization and analysed them by DIC microscopy (Figure 6C). Our results show that microtubules assembled in the presence of **1** and its derivatives show a similar morphology.

Finally, to investigate the effects of the compounds on microtubule organization in cells and, possibly, correlate these effects with their anti-proliferative activity, we have exposed MCF7 cells to **1-4** for 1 and 72 hours at concentrations corresponding to their IC_{50}.[18,19] At the end of the treatment, cells were fixed, microtubules stained with anti-α-tubulin antibodies and observed by fluorescence microscopy (Figure 7).

In control cells, we observed a widespread network of long microtubules other than the typical accumulation of microtubules at one side of the nucleus called the microtubule organizing centre (MTOC). Compound **1** induces the typical accumulation of microtubules in bundles at both 1 and 72 h of incubation times and a similar effect is evoked by **2**. On the contrary, compounds **3** and **4** appear to induce a more dramatic reorganization of the microtubules at early time points: cells appear roundish after 1 h of incubation with the above compounds and few bundles are detectable. To conclude, our in vitro results highlight that chemical modifications in derivatives **3** and **4** potentiate the well-known taxol ability to influence tubulin assembly kinetics by improving nucleation and elongation. In addition, these compounds evoked more severe effects on microtubule organization in MCF7 cells, in perfect agreement with our findings from the above reported computational study.

Conclusions.

The unbounded and bounded conformations of some biologically active 1,14-heterofused taxanes were investigated by MD simulations and results were compared to the known postulated bioactive conformation of paclitaxel. We evidenced that compounds **2-4** present unbounded geometries comparable to the T-taxol model and these conformations, herein referred as pseudo-T-Taxol, also resulted the most stable for the bounded

taxanes. Interestingly, although the amido-derivative **4** showed some deviation from the pseudo-T-taxol conformation and also the lowest computed binding affinity, it provided the highest stabilization of the α1-β2 interaction in a tubulin tetramer model, followed by compound **3**.

The different behaviour of **3** and **4** with respect to ortataxel **2**, also characterized by a 1,14-carbonyl bridge, might depends on the different physical-chemical features of the substituent at C14. Indeed, in compound **4** a strong hydrogen bond is formed between the carbamic nitrogen and the carboxy group of BOC in the side-chain. In **2** such an attractive interaction is replaced by a repulsion between the same group and the oxygen of the carbonate. Compound **3** lies in the middle between **2** and **4**, providing that the substitution of position 14 with methylidene does not cause a repulsive or an attractive interaction.

Biological data consolidate the computational outcomes and highlight the significant impact of the 1,14-heterofused taxanes **3** and **4** on tubulin kinetics and organization. As **3** and **4** speed up in vitro tubulin assembly by promoting the nucleation phase, these derivatives likely attest an improved ability to stabilize microtubules. Next, compounds **3** and **4** affect microtubule network in cell earlier than paclitaxel **1**. Although we cannot exclude that the precocious microtubule collapse observed in cells exposed to compounds **3** and **4** could be amplified by additional and not-microtubule dependant mechanisms, our data clearly show that chemical modifications in these derivatives augment paclitaxel performance in targeting tubulin organization in cell and, consequently, in inhibiting cell growth.

Experimental Section

Computational Methods. Conformational searches for **1**-**4** were done using low-mode molecular dynamics with the MMFF94x force field and Born solvation, as implemented in the MOE software.[16] The α,β-tubulin structure was obtained from the 1JFF crystal structure[15] by reconstructing missing residues through the homology model module implemented in MOE. The model was then protonated with the H++ server accordingly to a pH of 6.5 and a salinity of 0.15 M,[21] and then relaxed by a force field minimization (Amber force field implemented in MOE) with backbone restraints (tether atom = 1000). Docking were performed with MOE and two protocols well reproduced the paclitaxel binding conformation as found in 1JFF. Protocol 1, using the Triangle Matcher algorithm with default settings and London dG scoring function, followed by force field refinement (MMFF94x) of the poses and rescoring (London dG), provided the best matching with the T-taxol conformation for the first pose (r.m.s.d. = 0.81 Å). Protocol 2, using the Alpha Triangle algorithm (800000 and 5000000 for minimum and maximum iteration, respectively, timeout = 6000 seconds) and Affinity scoring function, followed by force field refinement and rescoring (Affinity), provided an r.m.s.d. = 1.83 Å for the first pose, but 0.81 and 1.00 Å for the second and third, respectively. Both protocols were chosen, the first because it produced the best fitting for the top-ranked pose, the second because it was able to find the highest number of low r.m.s.d. geometries within the top-five poses. The top-five poses of compounds 1-4 were then used to generate α,β-tubulin complexes for MD simulations. Analogue complexes were also prepared using the lowest energy conformation obtained by the previously described conformational search. All complexes were neutralized by adding 19 Na+ ions and solvated by a cubic TIP3P water box extending up to 10 Å from the solute. Orientation and conformation independent RESP charges were derived for ligands **1**-**4** using the REDIII procedure on two conformations and two orientations,[22] using the Gaussian03 software for ab-initio geometry optimization and molecular electrostatic potential calculation.[23] Parameters for GTP and GDP residues were downloaded from the Amber parameter database.[24] MD simulations were performed with the pmemd module of the Amber11 program package using the ff03 and gaff force fields.[25,26] All complexes were minimized, heated up to the final temperature of 300 K by six consecutive 50 ps runs in which backbone restraints were gradually released from 10 to 5 kcal/mol•Å and ligands restraints released from 5 to 0.5 kcal/mol•Å. These restraints were also kept for the following 100 ps equilibration in NVT ensemble and 100 ps in NPT ensemble, then were gradually reduced to 0 during the following 400 ps of NPT equilibration. A 2 ns production run was then conduced on the unrestrained systems. A cut-off for electrostatic of 8 Å, a time step of 0.002 ps and the SHAKE algorithm, constraining bonds involving hydrogens, were applied to all calculation.[27] The same protocol, extended to 4 ns of production run, was applied for the MD simulation of the 1β,1α-2β,2α tubulin tetramer (unbounded or bounded with **1**-**4**), obtained by superposing two units of the previously described dimers to the tubulin tetramer crystal structure 3N2G,[20] in order to preserve the taxol binding site. Geometrical analyses and MM-PBSA calculations (50 snapshots at regular intervals) were performed in all cases on the last ns of the production run. Both Generalized Born and Poisson Boltzmann methods were applied for evaluating the electrostatic contribution to solvation energy, obtaining comparable results (Table S1, Supporting Information). MD trajectory analyses were performed with both ptraj and VMD 1.8.5.[28]

Tubulin assembly assay. Tubulin was purified from bovine brain purchased from a local slaughterhouse, conserved before use in ice-cold PBS (20 mM Na-phosphate, 150 mM NaCl, pH 7.2) and used as soon as possible. Pure tubulin was obtained by two cycles of polymerization-depolymerization in a high-molarity buffer,[29] resuspended in BRB80 (80 mM K-Pipes pH 6.9, 2 mM EGTA, 1 mM $MgCl_2$), snap-frozen in aliquots in liquid nitrogen and kept at -80°C. Protein concentration was determined by MicroBCA assay kit (Pierce). Stock solutions of the drugs were prepared by dissolving the powers at a concentration of 5 mM in methanol. To assess their effects on tubulin assembly, bovine tubulin (1.3 mg/ml) was mixed with different compounds or an equal volume of the solvent (final 1% methanol) in an assembly buffer minus GTP (80 mM K-Pipes pH 6.9, 2 mM EGTA, 1 mM $MgCl_2$, 10% glycerol). The reaction mixtures (55 µl) were prepared at 0 °C, and each reaction was started by plating the cuvette at 37 °C in an Ultraspec 300 spectrophotometer (Pharmacia) equipped with a temperature controller. The kinetics of tubulin polymerisation were assessed by turbidimetry analysis following the increase in absorbance at 350 nm for 30 min. At least three independent experiments were performed with each compound.

Kinetic parameters of tubulin assembly. The reaction of

tubulin assembly has been analyzed to point out the potential effects of the selected compounds on the kinetic parameters defining its different phases: nucleation, elongation and steady state. Nucleation is a lag phase, during which a stable nucleus is forming, and allows microtubule polymerization. From nucleation phase we extrapolated the parameter *p* that represents the number of successive steps in the nucleation process by plotting $\log(A(t)/A_\infty)$ against $\log t$.[30] Elongation develops after the lag phase and is the phase during which the maximum extent of tubulin polymerization occurs following a procedure that is strongly similar to a first order chemical reaction.[31] At very initial elongation phase, one can extrapolate the maximal velocity of polymerization (V_i), as the variation of mass during time (dA/dt). Finally, steady state is the terminal phase during which the total amount of microtubules does not change because the rates of microtubule growth and shortening are identical. We extrapolate the steady state extent of assembly (ΔA) as the absorbance maximum obtained at the plateau of the kinetics curve minus the absorbance measured at the initial elongation phase.

Differences between the effects of the different compounds on *p* value, V_i and ΔA were evaluated by ANOVA followed by Dunnett post hoc test.

DIC microscopy. At the end of the assembly assay, microtubules were collected by centrifugation at 30,000*g* for 30 min at 30 °C, fixed with 0.5% glutaraldehyde in the assembly buffer (80 mM K-Pipes pH 6.9, 2 mM EGTA, 1 mM $MgCl_2$, 10% glycerol), and put onto coverslips. Image acquisition was performed using a Zeiss Axiovert 200 equipped with differential interference contrast (DIC) optics, a 63× oil objective, and a digital image recording system (Axiocam HRM Rev. 2 camera driven by Axiovision software rel. 4.4, Zeiss).

Cell culture and immunofluorescence analyses. Microtubule organization in cell was revealed by indirect immunofluorescence (IF) analyses. Human breast adenocarcinoma cell line MCF7 (HTB-22; American Type Culture Collection, Rockville, MD, U.S.A.) was grown in minimal essential medium with Earle's (E-MEM), supplemented with 10% fetal bovine serum (Hyclone Europe, Oud-Beijerland, Holland), 2 mM L-glutamine, 100 U/ml penicillin and non-essential amino acids. Cells were maintained at 37 °C in a humidified atmosphere at 5% CO_2. Experiments were carried out with cells plated on glass coverslips at a density of 1.0×10^4 cells/cm^2 and grown for 24 h in control medium following an incubation of 1h and 72 h in the presence of the drugs (final concentration corresponding to the IC_{50} previously determined by proliferation assay)[18,19] or solvent vehicle alone (methanol) diluited 1:1000 in the culture medium. At the end of the treatments, cells were fixed and stained as previously described.[32] Briefly, MCF7 cells were fixed and permeabilized for 6 min with methanol at –20 °C, washed with PBS and blocked in PBS + 5% bovine serum albumin (BSA) for 15 min at room temperature. To localize tubulin, the cells were incubated with monoclonal anti α-tubulin antibody (clone B-5-1-2, Sigma-Aldrich), 1:500 in PBS for 1 h at 37 °C. As secondary antibodies we used goat anti-mouse Alexa Fluor™ 568 (Molecular Probes), 1:1000 in PBS + 1% BSA for 45 min at 37 °C. Nuclei staining was performed by incubation with DAPI (0.25 μg/ml in PBS) for 15 min at room temperature. The coverslips were mounted in Mowiol® (Calbiochem)–DABCO (Sigma-Aldrich) and examined with a Zeiss Axiovert 200 microscope equipped with a 63× Neofluor lens. Images were acquired with an Axiocam camera (Zeiss) and PC running Axiovision software (Zeiss).

Acknowledgements

We thank the "Consorzio Interuniversitario Lombardo per L'Elaborazione Automatica" (CILEA) for computational facilities. D.C. was supported by "Dote ricerca", FSE, Regione Lombardia.

Notes and references

[a] *Dipartimento di Scienze Farmaceutiche - sezione di Chimica Generale e Organica "Alessandro Marchesini", Università degli Studi di Milano, via Venezian, 21 20133 Milano, Italy. Fax: +39 02 50314476; Tel: +39 02 50314480; E-mail: alessandro.contini@unimi.it*

[b] *Dipartimento di Bioscienze, Università degli Studi di Milano, via Celoria, 26 20133 Milano, Italy*

[c] *Indena SPA, viale Ortles 12, 20139 Milano, Italy*

‡ *These authors equally contributed to this work.*

† *Electronic Supplementary Information (ESI) available: further computational and experimental details, extended tables, energies, Cartesian coordinates of the most stable geometries obtained for the unbounded ligands. See DOI: 10.1039/b000000x/*

1 M. C. Wani, H. I. Taylor, M. E. Wall, P. Coggon, A. T. McPhail, *J. Am. Chem. Soc*., 1971, **93**, 2325.

2 F. Gueritte-Voegelein, D. Guenard, F. Lavelle, M. -T. Le Goff, I. Mangatal, P. Potier, *J. Med. Chem.*, 1991, **34**, 992.

3 D. G. I. Kingston, *J. Nat. Prod.*, 2000, **63**, 726 and references cited therein.

4 I. Ojima, J. C. Slater, S. D. Kuduk, C. S. Takeuchi, R. H. Gimi, C. M. Sun, Y. H. Park, P. Pera, J. M.Veith, R. J. Bernacki, *J. Med. Chem.*, 1997, **40**, 267.

5 M. Beer, L. Lenaz, D. Amadori, Ortataxel Study Group, *J. Clin. Oncol.*, 2008, 26, May 20 suppl, abstr 1066.

6 a) A. Battaglia, E. Baldelli, E. Bombardelli, G. Carenzi, G. Fontana, M. L. Gelmi, A. Guerrini, D. Pocar, *Tetrahedron*, 2005, **61**, 7727. b). E. Baldelli, A. Battaglia, E. Bombardelli, G. Carenzi, G. Fontana, M. L. Gelmi, A. Guerrini, D. Pocar, *J. Org. Chem*., 2004, **69**, 6610. c) E. Baldelli, A. Battaglia, E. Bombardelli, G. Carenzi, G. Fontana, A. Gambini, M. L. Gelmi, A. Guerrini, D. Pocar, *J. Org. Chem.*, 2003, **68**, 9773.

7 a) J. Dubois, F. Guerritte-Voeglein, N. Guedira, P. Potier, B. Gilet, J. -C. Betoeil, *Tetrahedron*, 1993, *49*, 6533. b) H. J. Williams, A. I. Scott, R. A. Dieden, C. S. Swindell, L. E. Chirlian, M. M. Francl, J. M. Heerding, N. E. Krauss, *Can. J. Chem.*, 1994, **72**, 252. c) R. E. Cachau, R. Gussio, J. A. Beutler, G. N. Chmurny, B. D. Hilton, G. M. Muschik, J. W. Erickson, *Int. J. Supercomput. Appl. High Perform. Comput.*, 1994, **8**, 24.

8 a) D. G. Vander Velde, G. I. Georg, G. L. Grunewald, C. W. Gunn, L. A. Mitscher, *J. Am. Chem. Soc.*, 1993, **115**, 11650. b) L. G. Paloma, R. K. Guy, W. Wrasidlo, K. C. Nicolau, *Chem. Biol.*, 1994, *1*, 107. c) I. Ojima, S. D. Kuduk, S. Chakravarty, M. Ourevitch, J. -P. Begue, *J. Am. Chem. Soc.*, 1997, **119**, 5519. d) I. Ojima, S. Chakravarty, S. Lin, L. He, S. B. Horwitz, S. D. Kuduk, S. J. Danishefsky, *Proc. Natl. Acad. Sci. U.S.A.*, 1999, **96**, 4256.

9 a) L. Barboni, C. Lambertucci, G. Appendino, D. G. Vander Velde, R. H. Himes, E. Bombardelli, M. Wang, J. P. Snyder, *J. Med. Chem.* 2001, **44**, 1576. b) T. C. Boge, Z. -J. Wu, R. H. Himes, D. G. Vander Velde, G. I. Georg, *Bioorg. Med. Chem. Lett.*, 1999, **9**, 3047. c) I. Ojima, S. Lin, T. Inoue, M. L. Miller, C. P. Borella, X. Geng, J. J. Walsh, *J. Am. Chem. Soc.*, 2000, **122**, 5343. d) I. Ojima, X. Geng, S. Lin, P. Pera, R. J. Bernacki, *Bioorg. Med. Chem. Lett.*, 2002, **12**, 349-352. e) X. Geng, M. L. Miller, S. Lin, I. Ojima, *Org. Lett.*, 2003, **5**, 3733. f) O. Querolle, J. Dubois, S. Thoret, C. Dupont, F. Guéritte, D. Guénard, *Eur. J. Org. Chem*., 2003, 542. g) O. Querolle, J. Dubois, S. Thoret, F. Roussi, S. Montiel-Smith, F. Guéritte, D. Guénard, *J. Med. Chem.*, 2003, **46**, 3623, h) O. Querolle, J. Dubois, S. Thoret, F.

Roussi, F. Guéritte, D. Guénard, *J. Med. Chem.*, 2004, **47**, 5937. i) R. Geney, L. Sun, P. Pera, R. J. Bernacki, S. Xia, S. B. Horwitz, C. L. Simmerling, I. Ojima, *Chem. Biol.*, 2005, **12**, 339.

10 a) T. Ganesh, R. C. Guza, S. Bane, R. Ravindra, N. Shaker, A. S. Lakdawala, J. P. Snyder, D. G. I. Kingston, *Proc. Nat. Ac. Sci.*, 2004, **101**, 10006. c) S. Tang, C. Yang, P. Brodie, S. Bane, R. Ravindra, S. Sharma, Y. Jiang, J. P. Snyder, D. G. I. Kingston, *Org. Lett.*, 2006, **8**, 3983. d) T. Ganesh, C. Yang, A. Norris, T. Glass, S. Bane, R. Ravindra, A. Banerjee, B. Metaferia, S. L. Thomas, P. Giannakakou, A. A. Alcaraz, A. S. Lakdawala, J. P. Snyder, D. G. I. Kingston, *J. Med. Chem.*, 2007, **50**, 713.

11 a) J. P. Snyder, J. H. Nettles, B. Cornett, K. H. Downing, E. Nogales, *Proc. Nat. Ac. Sci.*, 2001, **98**, 5312-5316. b) A. A. Alcaraz, A. K. Mehta, S. A. Johnson, J. P. Snyder, *J. Med. Chem.*, 2006, **49**, 2478. c) Y. Paik, C. Yang, B. Metaferia, S. Tang, S. Bane, R. Rudravajhala, N. Shanker, A. A. Alcaraz, S. A. Johnson, J. Schaefer, R. D. O'Connor, L. Cegelski, J. P. Snyder, D. G. I. Kingston, *J. Am. Chem. Soc.*, 2007, **129**, 361.

12 M. Magnani, F. Ortuso, S. Soro, S. Alcaro, A. Tramontano, M. Botta, *FEBS J.*, 2006, **273**, 3301.

13 A. Mitra, D. Sept, *Biophys. J.*, 2008, *95*, 3252.

14 S. Pieraccini, G. Saladino, G. Cappelletti, D. Cartelli, P. Francescato, G. Speranza, P. Manitto, M. Sironi, *Nature Chemistry*, 2009, **1**, 642.

15 J. Löwe,; H. Li, K. H. Downing, E. Nogales, *J. Mol. Biol.*, 2001, **313**, 1045-1057.

16 MOE 2010.10, http://www.chemcomp.com/

17 a) J. Wang, P. Morin, W. Wang, P. A. Kollman, *J. Am. Chem. Soc.*, 2001, **123**, 5221. b) N. Ferri, A. Corsini, P. Bottino, F. Clerici, A. Contini, *J. Med. Chem.*, 2009, **52**, 4087.

18 I. Ojima, Y. H. Park, C. Sun, I. Fenoglio, G. Appendino, P. Pera, R. J. Bernacki, *J. Med. Chem.*, 1994, **37**, 1408.

19 a) G. Fontana, A. Battaglia, M. L. Gelmi, E. Baldelli, G. Carenzi, E. Bombardelli, C. Manzotti, R. J. Bernacki, SAR of 14-Substituted Taxanes. 228th ACS National Meeting, Philadelphia, PA, August 22-26, 2004 Abstract MEDI #99. b) See Supporting Information for experimental details.

20 P. Barbier, A. Dorleans, F. Devred, L. Sanz, D. Allegro, C. Alfonso, M. Knossow, V. Peyrot, J. M. Andreu, *J. Biol. Chem.*, 2010, **285**, 31672.

21 J. C. Gordon, J. B. Myers, T. Folta, V. Shoja, L. S. Heath, A. Onufriev, *Nucleic Acids Res.*, 2005, **33**, W368.

22 F. -Y. Dupradeau, A. Pigache, T. Zaffran, C. Savineau, R. Lelong, N. Grivel, D. Lelong, W. Rosanski, P. Cieplak, *Phys. Chem. Chem. Phys.*, 2010, **12**, 7821.

23 Gaussian 03, Revision B.04, M. J. Frisch et al. Gaussian, Inc., Wallingford CT, 2004.

24 R. Bryce, http://www.pharmacy.manchester.ac.uk/bryce/amber/

25 D. A. Case, T. Cheatham, T. Darden, H. Gohlke, R. Luo, K. M. Merz, A. Onufriev, C. Simmerling, B. Wang, R. Woods, *J. Comput. Chem.*, 2005, **26**, 1668.

26 J. Wang, R. M. Wolf, J. W. Caldwell, P. A. Kollman, D. A. Case, *J. Comput. Chem.*, 2004, **25**, 1157.

27 J. -P. Ryckaert, G. Ciccotti, H. J. C. Berendsen, *J. Comput. Phys.*, 1977, **23**, 327.

28 W. Humphrey, A. Dalke, K. Schulten, *J. Mol. Graph.*, 1996, **14**, 33.

29 M. Castoldi, A. V. Popov, *Proein Expr. Purif.*, 2003, **32**, 83-88.

30 H. Flyvbjerg, E. Jobs, S. Leibler, *Proc. Natl. Acad. Sci. USA*, 1996, **93**, 5975-5979.

31 K. A. Johnson, G. G. Borisy, *J. Mol. Biol.*, 1977, **117**, 1.

32 G. Cappelletti, M. G. Maggioni, R. Maci, *J. Neurosci. Res.*, 1999, **56**, 28.